COMPLEX DYNAMICS AND MULTISTABILITY IN NONLINEAR RESONANT NANOSYSTEMS BEYOND THE DUFFING CRITICAL AMPLITUDE

N. Kacem*[1]

[1]FEMTO-ST Institute - UMR 6174, CNRS-UFC-ENSMM-UTBM
24, chemin de l'Épitaphe, F-25000 Besançon, France
najib.kacem@femto-st.fr

Keywords: Nonlinear Dynamics, Nanotechnology, Multistability, Complex Dynamics.

Abstract. *Analytical multi-physics models which include main sources of nonlinearities for nanoresonators electrostatically actuated are developed in order to assess complex dynamics in nanosystems beyond the Duffing critical amplitude. In particular, multistability is investigated for doubly clamped beams and cantilevers. The bifurcation topology of a particular multistable behavior (up to five amplitudes for a given frequency) is parametrically identified and experimentally validated.*

1 INTRODUCTION

Micro and nanoelectromechanical (MEMS/NEMS) devices have been the subject of extensive research for a number of years and have generated much excitement as their use in commercial applications has increased. Indeed, MEMS technology has opened up a wide variety of potential applications not only in the inertial measurement sector, but also spanning areas such as communications (filters, relays, oscillators, LC passives, optical switches), biomedicine (point-of-care medical instrumentation, microarrays for DNA detection and high throughput screening of drug targets, immunoassays, in-vitro characterization of molecular interactions), computer peripherals (memory, new I/O interfaces, read-write heads for magnetic disks) and other miscellaneous areas such as in projection displays, gas detection and mass flow detection.

NEMS are the natural successor to MEMS as the size of the devices is scaled down to the submicron domain. This transition is well adapted with the resonant sensing technique for a large panel of applications. One reason of down scaling resonant sensors to the NEMS size is the ability to detect very small physical quantities by increasing their sensitivity [1]. In particular, NEMS have been proposed for use in ultrasensitive mass detection [2, 3], radio frequency (RF) signal processing [4, 5], and as a model system for exploring quantum phenomena in macroscopic systems [6, 7].

Unfortunately, the nonlinear regime for nanomechanical resonators is easily reachable, so that the useful linear dynamic range of the smallest NEMS devices is severely limited. In fact, many applications we are hoping for in the near future will involve operation in the nonlinear regime, where the response to the stimulus is suppressed and frequency is pulled away from the original resonant frequency. Actually, it is a challenge to achieve large-amplitude motion of NEMS resonators without deteriorating their frequency stability [8]. The relative frequency noise spectral density [9] of a NEMS resonator is given by:

$$S_f = \left(\frac{1}{2Q}\right)^2 \frac{S_x}{P_0} \tag{1}$$

where S_x is the displacement spectral density and P_0 is the displacement carrier power, ie the RMS drive amplitude of the resonator $\frac{1}{2}A^2$. Remarkably, driving the resonator at large oscillation amplitude leads to better SNR and, thus, simplifies the design of the electronic feedback loop. However, doing so in the nonlinear regime reduces the sensor performances since the frequency instability of a nonlinear resonator is proportional to its oscillation amplitude. Moreover, even when NEMS resonators are used as oscillators in closed-loop, a large part of noise mixing [10, 11] due to nonlinearities drastically reduces their dynamic range and alters their detection limit.

This paper is about investigating such limitations beyond the Duffing critical amplitude [12, 13], based on the nonlinear dynamics of nanomechanical resonators. In particular, multistability is tracked analytically and experimentally for clamped-clamped nanobeams and nanocantilevers showing a complex multistable dynamics with up to five amplitudes for a given frequency.

2 MODELS

2.1 Clamped-clamped beam resonators

A clamped-clamped nanobeam is considered (Figure 1) subject to a viscous damping with coefficient $\tilde{c}$ per unit length and actuated by an electric load $v(t) = V_{dc} + V_{ac}\cos(\tilde{\Omega}\tilde{t})$, where V_{dc} is the DC polarization voltage, V_{ac} is the amplitude of the applied AC voltage, and $\tilde{\Omega}$ is the excitation frequency.
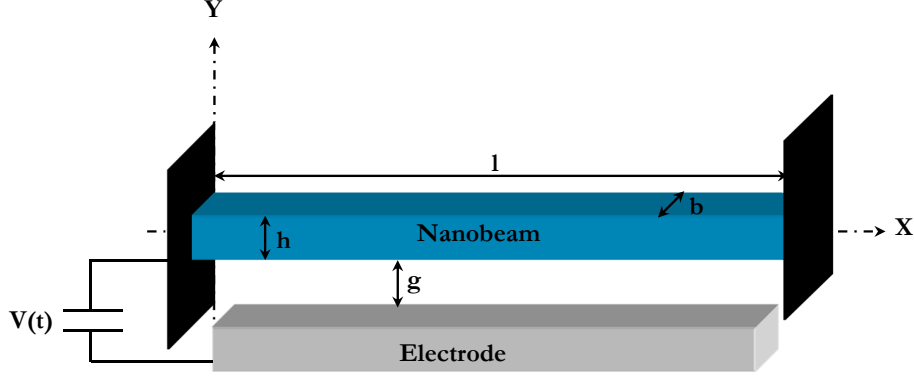
Figure 1: Schema of an electrostatically actuated clamped-clamped nanobeam

2.1.1 Equation of motion

The equation of motion that governs the transverse deflection $w(x, t)$ is written as:

$$EI\frac{\partial^4 \tilde{w}(\tilde{x}, \tilde{t})}{\partial \tilde{x}^4} + \rho bh\frac{\partial^2 \tilde{w}(\tilde{x}, \tilde{t})}{\partial \tilde{t}^2} + \tilde{c}\frac{\partial \tilde{w}(\tilde{x}, \tilde{t})}{\partial \tilde{t}} - \left[\tilde{N} + \frac{Ebh}{2l}\int_0^l \left[\frac{\partial \tilde{w}(\tilde{x}, \tilde{t})}{\partial \tilde{x}}\right]^2 d\tilde{x}\right]\frac{\partial^2 \tilde{w}(\tilde{x}, \tilde{t})}{\partial \tilde{x}^2} =$$
$$\frac{1}{2}\varepsilon_0\frac{b\left[Vdc + Vac\cos(\tilde{\Omega}\tilde{t})\right]^2}{(g - \tilde{w}(\tilde{x}, \tilde{t}))^2} \quad (2)$$

where $\tilde{x}$ is the position along the nanobeam length, E and I are the Young's modulus and moment of inertia of the cross section. $\tilde{N}$ is the applied tensile axial force due to the residual stress on the silicon or the effect of the measurand, $\tilde{t}$ is time, ρ is the material density, h is the nanobeam thickness, g is the capacitor gap width, and ε_0 is the dielectric constant of the gap medium. The last term in Equation (2) represents an approximation of the electric force assuming a complete overlap of the area of the nanobeam and the stationary electrode. The boundary conditions of Equation (2) are:

$$\tilde{w}(0, \tilde{t}) = \tilde{w}(l, \tilde{t}) = \frac{\partial \tilde{w}}{\partial \tilde{x}}(0, \tilde{t}) = \frac{\partial \tilde{w}}{\partial \tilde{x}}(l, \tilde{t}) = 0 \quad (3)$$

2.1.2 Normalization

For convenience and equations simplicity, we introduce the nondimensional variables:

$$w = \frac{\tilde{w}}{g}, \quad x = \frac{\tilde{x}}{l}, \quad t = \frac{\tilde{t}}{\tau} \quad (4)$$

where $\tau = \frac{2l^2}{h}\sqrt{\frac{3\rho}{E}}$. The substitution of Equation (4) into Equations (2) and (3) leads to:

$$\frac{\partial^4 w}{\partial x^4} + \frac{\partial^2 w}{\partial t^2} + c\frac{\partial w}{\partial t} - \left[N + \alpha_1\int_0^1 \left[\frac{\partial w}{\partial x}\right]^2 dx\right]\frac{\partial^2 w}{\partial x^2} = \alpha_2\frac{[Vdc + Vac\cos(\Omega t)]^2}{(1 - w)^2} \quad (5)$$

$$w(0, t) = w(1, t) = \frac{\partial w}{\partial x}(0, t) = \frac{\partial w}{\partial x}(1, t) = 0 \quad (6)$$

3

The parameters appearing in Equation (5) are:

$$c = \frac{\tilde{c}l^4}{EI\tau} \quad N = \frac{\tilde{N}l^2}{EI} \quad \alpha_1 = 6\left[\frac{g}{h}\right]^2 \quad \alpha_2 = 6\frac{\varepsilon_0 l^4}{Eh^3 g^3} \quad \Omega = \tilde{\Omega}\tau \tag{7}$$

2.1.3 Solving

The total beam displacement $w(x,t)$ is a sum of a static dc displacement $w_s(x)$ and a time-varying ac displacement $w_d(x,t)$. However, for our devices, it is easy to check that the static deflexion is negligible. Typically, the measured quality factors Q are in the range of $10^4 - 5.10^4$ and the $Vdc \leq 200Vac$. Thus, the ratio between the static and the dynamic deflection is:

$$\frac{w_s(x)}{w_d(x,t)} \approx \frac{Vdc}{2Q.Vac} \leq 1\% \tag{8}$$

A reduced-order model is generated by modal decomposition transforming Equation (5) into a finite-degree-of-freedom system consisting of ordinary differential equations in time. We use the undamped linear mode shapes of the straight nanobeam as basis functions in the Galerkin procedure. To this end, we express the deflection as :

$$w(x,t) = \sum_{k=1}^{N_m} a_k(t)\phi_k(x) \tag{9}$$

where N_m is the number of modes retained in the solution, $a_k(t)$ is the kth generalized coordinate and $\phi_k(x)$ is the kth linear undamped mode shape of the straight nanobeam, normalized such that $\int_0^1 \phi_k\phi_j = \delta_{kj}$ where $\delta_{kj} = 0$ if $k \neq j$ and $\delta_{kj} = 1$ if $k = j$.

The modal basis is formed of the eigenmodes of a linear undamped straight nanobeam. The latter are the solutions of the following equation:

$$\frac{d^4\phi_k(x)}{dx^4} = \lambda_k^4 \phi_k(x) \tag{10}$$

We multiply Equation (5) by $\phi_k(x)(1-w)^2$ in order to include the complete contribution of the nonlinear electrostatic forces in the resonator dynamics without approximation. Next, we substitute Equation (9) into the resulting equation, use Equation (10) to eliminate $\frac{d^4\phi_k(x)}{dx^4}$, integrate the outcome from $x = 0$ to 1, and obtain a system of coupled ordinary differential equations in time.

Since the first mode is the dominant mode of the system and the higher modes are negligible, it is enough to consider $n = 1$ [14] and obtain:

$$\ddot{a}_1 + (500.564 + 12.3N)a_1 + (927 + 28N + 151\alpha_1)a_1^3 + 347\alpha_1 a_1^5$$
$$+ (1330.9 + 38.3N)a_1^2 + 471\alpha_1 a_1^4 + 2.66c_1 a_1 \dot{a}_1 + 1.85c_1 a_1^2 \dot{a}_1$$
$$+ c_1 \dot{a}_1 + 2.66a_1 \ddot{a}_1 + 1.85a_1^2 \ddot{a}_1 = -\frac{8}{3\pi}\alpha_2 \left[Vdc + Vac\cos(\Omega t)\right]^2 \tag{11}$$

In addition, since near-resonant behavior is the principal operating regime of the proposed system, a detuning parameter, σ is introduced, as given by:

$$\Omega = \omega_1 + \varepsilon\sigma \tag{12}$$

Separating the resulting equations and averaging them over the period $\frac{2\pi}{\Omega}$ in the t-domain results in the system's averaged equations, in terms of amplitude and phase, which are given by:

$$\dot{A} = -\frac{1}{2}\epsilon\xi_0 A - \frac{1}{8}\epsilon\xi_2 A^3 + \frac{1}{2}\epsilon\frac{\kappa}{\omega_1}\sin\beta + O(\varepsilon^2) \tag{13}$$

$$A\dot{\beta} = -A\sigma\epsilon + \frac{3}{8}\epsilon\frac{\chi_3}{\omega_1}A^3 + \frac{5}{16}\epsilon\frac{\chi_5}{\omega_1}A^5 - \frac{7}{10}\epsilon\omega_1 A^3 + \frac{1}{2}\epsilon\frac{\kappa}{\omega_1}\cos\beta + O(\varepsilon^2) \tag{14}$$

where $\omega_1 = \sqrt{500.564 + 12.3N}$, $\xi_0 = c_1$, $\xi_2 = 1.85c_1$, $\chi_3 = 927 + 28N + 151\alpha_1$, $\chi_5 = 347\alpha_1$ and $\kappa = \frac{16}{3\pi}\alpha_2 VacVdc$.

2.2 Cantilevers

In order to develop a model for nanocantilever beams, a slender uniform flexible beam is considered as shown in Figure 2. The beam is initially straight and it is clamped at one end and free at the other end, subject to viscous damping with a coefficient $\tilde{c}$ per unit length and actuated by an electric load $v(t) = V_{dc} + V_{ac}\cos(\tilde{\Omega}\tilde{t})$, where V_{dc} is the DC polarization voltage, V_{ac} is the amplitude of the applied AC voltage, $\tilde{t}$ is time and $\tilde{\Omega}$ is the excitation frequency. In addition, the beam follows the Euler-Bernoulli beam theory, where shear deformation and rotary inertia terms are negligible. In order to derive the nonlinear equation of motion describing the flexural
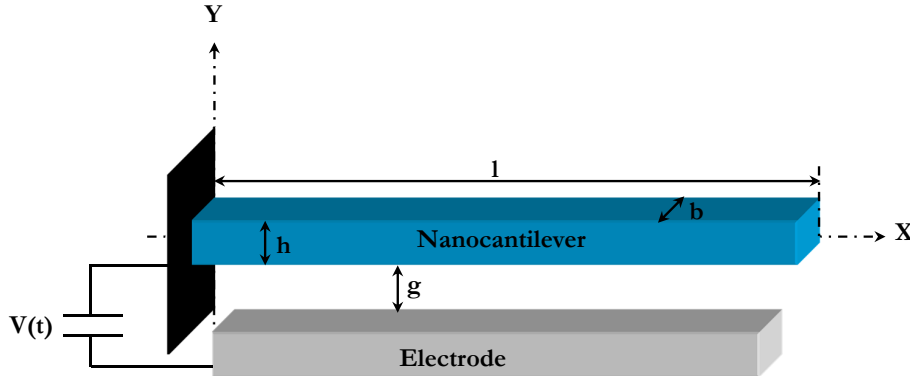

Figure 2: Schema of an electrostatically actuated nanocantilever

vibration of a cantilever beam electrostatically actuated, we follow a variational approach, based on the extended Hamilton principle and used by Crespo da Silva and Glynn [15, 16] and Crespo da Silva [17, 18].

$$EI\left\{\tilde{w}'''' + \left[\tilde{w}'\left(\tilde{w}'\tilde{w}''\right)'\right]'\right\} + \rho bh\ddot{\tilde{w}} + \tilde{c}\dot{\tilde{w}} =$$

$$-\frac{1}{2}\rho bh\left\{\tilde{w}'\int_l^{\tilde{x}}\left[\frac{\partial^2}{\partial\tilde{t}^2}\int_0^{s_1}(\tilde{w}')^2 ds_2\right]ds_1\right\}' + \frac{1}{2}\varepsilon_0\frac{b\left[V_{dc} + V_{ac}\cos(\tilde{\Omega}\tilde{t})\right]^2}{(g - \tilde{w})^2} \tag{15}$$

where primes and dots denote respectively the partial differentiation with respect to the arclength $\tilde{x}$ and to the time $\tilde{t}$. $\tilde{w}$ is the beam bending deflection, E and I are the Young's modulus and geometrical moment of inertia of the cross section. l and b are the length and width of the

nanobeam, ρ is the material density, h is the nanobeam thickness in the direction of vibration, g is the capacitor gap width, and ε_0 is the dielectric constant of the gap medium.

The first term in the left-hand side of Equation (15) is due to the nonlinear expression for the curvature of the beam, while the first term in the right-hand side, which involves a double time derivative, is the nonlinear inertial term. The boundary conditions are:

$$\tilde{w}(0,\tilde{t}) = \tilde{w}'(0,\tilde{t}) = \tilde{w}''(l,\tilde{t}) = \tilde{w}'''(l,\tilde{t}) = 0 \tag{16}$$

Substituting Equation (4) into Equations (15) and (16), we obtain:

$$w^{iv} + \ddot{w} + c\dot{w} + \delta_1 \left[w' \left(w'w'' \right)' \right]' =$$

$$-\delta_2 \left\{ w' \int_1^x \left[\frac{\partial^2}{\partial t^2} \int_0^{x_1} (w')^2 dx_2 \right] dx_1 \right\}' + \delta_3 \frac{V_{dc}}{V_{ac}} \frac{\left[1 + \frac{V_{ac}}{V_{dc}} \cos(\Omega t) \right]^2}{(1-w)^2} \tag{17}$$

$$w(0,t) = w'(0,t) = w''(1,t) = w'''(1,t) = 0 \tag{18}$$

where primes and dots denote respectively the partial differentiation with respect to the dimensionless arclength x and to the dimensionless time t. The parameters appearing in Equations (17) are:

$$c = \frac{\tilde{c}l^4}{EI\tau}, \quad \delta_1 = \left[\frac{g}{l} \right]^2, \quad \delta_2 = \frac{1}{2} \left[\frac{g}{l} \right]^2$$

$$\delta_3 = 6 V_{ac} V_{dc} \frac{\varepsilon_0 l^4}{Eh^3 g^3}, \quad \Omega = \tilde{\Omega}\tau \tag{19}$$

The electrostatic force in Equation (17) is expanded in a fifth order Taylor series, in order to capture 5 possible amplitudes for a given frequency in the mixed behavior [19]. Then, Equation (9) is substituted into the resulting equation, Equation (10) is used to eliminate $\dfrac{d^4\phi_k(x)}{dx^4}$, and the outcome is multiplied by ϕ_k and integrated from $x = 0$ to 1 for $k \in [1,n] \cap N$. Thus, a system of coupled ordinary differential equations in time is obtained.

In addition, since near-resonant behavior is the principal operating regime of the proposed system, a detuning parameter σ is introduced, as given by:

$$\Omega = \omega_1 + \varepsilon\sigma \tag{20}$$

where $\omega_1 = \sqrt{\lambda_1^2 - \frac{V_{ac}}{V_{dc}}\delta_3 - 2\frac{V_{dc}}{V_{ac}}\delta_3}$ and ε is the small nondimensional bookkeeping parameter. Separating the resulting equations and averaging them over the period $\frac{2\pi}{\Omega}$ in the t-domain results in the system's averaged equations in terms of amplitude A and phase β given by:

$$\dot{A} = \frac{\varepsilon\delta_3 \sin\beta}{\omega_1} \left(0.78 + 1.11A^2 + 2.44A^4 \right) - \frac{\varepsilon c}{2} A + O(\varepsilon^2) \tag{21}$$

$$\dot{\beta} = \varepsilon\sigma - \varepsilon\frac{\delta_3 \cos\beta}{\omega_1} \left(\frac{0.78}{A} + 3.32A + 12.19A^3 \right) + \varepsilon\frac{A^4\delta_3}{\omega_1} \left(12.51\frac{V_{dc}}{V_{ac}} - 6.25\frac{V_{ac}}{V_{dc}} \right)$$

$$-\varepsilon\frac{15.16A^2\delta_1}{\omega_1} + \frac{\varepsilon\delta_3 A^2}{\omega_1} \left(1.76\frac{V_{ac}}{V_{dc}} + 3.52\frac{V_{dc}}{V_{ac}} \right) + 2.3\varepsilon A^2\delta_2\omega_1 + O(\varepsilon^2) \tag{22}$$

3 NUMERICAL SIMULATIONS

The steady-state motions occur when $\dot{A} = \dot{\beta} = 0$, which corresponds to the singular points of Equations (13) and (14) or (21) and (22). Thus, the frequency response equation can be written in its parametric form $A = K_1(\beta), \Omega = K_2(\beta)$ as a function of the phase β. This set of two equations is easily implementable in Matlab or Mathematica. This ability makes the model suitable for NEMS designers as a quick tool to optimize the resonant sensors performance.
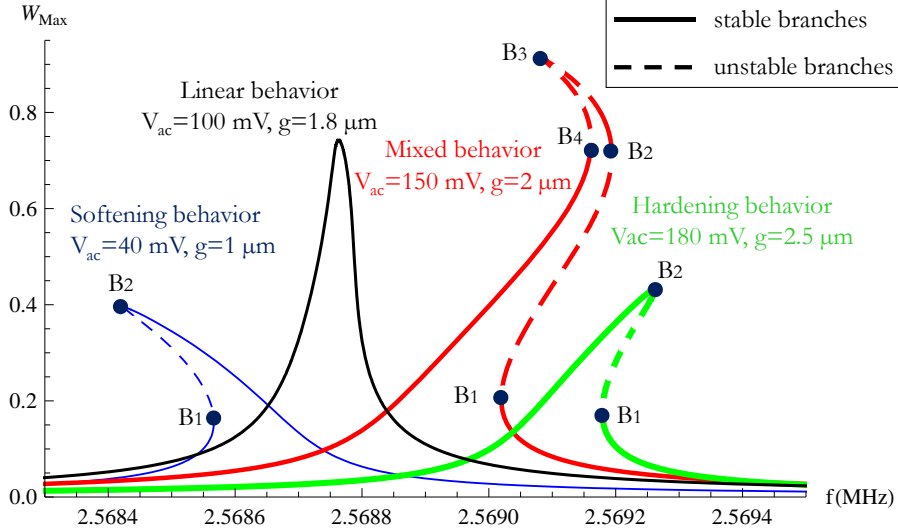

Figure 3: Analytical forced frequency responses for $Q = 10^4$ and several values of g and V_{ac}. W_{max} is the beam displacement at its free end normalized by the gap g. The different bifurcation points are $\{B_1, B_2, B_3, B_4\}$, the point B_4 characterizes the initiation of the mixed behavior.

The plots of Figure 3 were carried out for a resonant nano-cantilever with the following set of parameters: $l = 12.5 \mu m$, $h = 300 nm$, $b = 500 nm$ and $V_{dc} = 50 V_{ac}$. g and V_{ac} were used for parametric studies. This analytical model enables the capture of all the nonlinear regimes in the resonator dynamics and describes the competition between the mechanical hardening and the electrostatic softening behaviors.

Practically, when $h/g << 1$ and for a high quality factor, the dynamics is dominated by the hardening nonlinearities and in the opposite case, the frequency response is nonlinearly softening. Between these two configurations ($h/g = 0.15$ for instance), a mixed hardening-softening behavior is inescapable. This leads to a multistability with five possible amplitudes for a given frequency. It is highly unstable and difficult to control for NEMS designers.

4 EXPERIMENTAL VALIDATION

The device consists in a silicon doubly clamped beam electrostatically in plane actuated and detected using two electrodes which allows for 2 port electric measurements. The resonator is $200 \mu m$ long, $4 \mu m$ thick, $2 \mu m$ wide, the actuation gap is $1 \mu m$, and the detection gap $750 nm$. The device was placed in a vacuum chamber, and the electrical measurements were performed at room temperature using a low noise lock-in amplifier. The drive voltage is $V_{ac} = 0.6 V$ and the beam is polarized with $V_{dc} = 10 V$. Figure 4 shows the frequency response of the device, with up- and down- sweeps. The quality factor obtained with this polarization voltage and in a linear regime is 4000. The Duffing critical amplitude is then $A_c = 53 nm$, *i.e.* $V_c = 25 \mu V$. The

peak obtained is then far beyond A_c, up to 70% of the gap. The frequency response shows 4 bifurcation points noted B_i, at which jumps J_i occur to destination points D_i on stable branches, according to the direction of the sweep : as the frequency is swept up from f_0, the output voltage follows the path labelled $f_0 - B_4 - D_4 - B_2 - D_2 - f_1$, and as it is swept down from f_1, the path $f_1 - B_1 - D_1 - B_3 - D_3 - f_0$ is followed. In the presence of the 3 other bifurcation points, the point B_4 may be called the mixed behavior initiation point. It is highly unstable: it is located at relatively high amplitude (*i.e.* in a state of high potential energy) as opposed to point B_1 or as opposed to a typical softening behavior, and the state variables have to jump to a destination stable branch at even higher amplitude.

The parametric analytical frequency response is superposed to the experimental points in Figure 4. The model shows an excellent agreement: the 4 bifurcation points exist and are well located, and the stable branches coincide very well with the measurement. This confirms the performance and the accuracy of the model at high amplitude in the nonlinear regime.
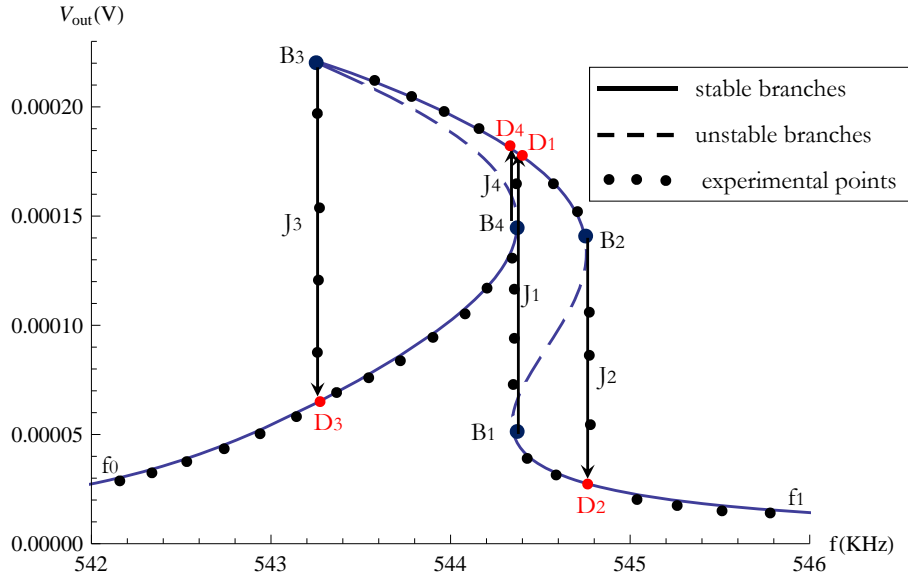

Figure 4: Analytical and experimental frequency curves showing a mixed behavior and the followed paths respectively in a sweep up frequency $f_0-B_4-D_4-B_2-D_2-f_1$ and a sweep down frequency $f_1-B_1-D_1-B_3-D_3-f_0$. $\{J_1, J_2, J_3, J_4\}$ are the four jumps cauterizing a typical mixed behavior of NEMS resonators, $\{B_1, B_2, B_3, B_4\}$ are the different bifurcation points and $\{D_1, D_2, D_3, D_4\}$ are the destination points after jumps. The two branches $[B_1, B_2]$ and $[B_3, B_4]$ in dashed lines are unstable.

5 CONCLUSIONS

Analytical models have been developed to quantitatively assess the nonlinear dynamics of NEMS resonators. These models include the main sources of nonlinearities (electrostatic, geometric and inertial) and they are based on the modal decomposition (the Galerkin discretization) combined with a perturbation technique (the averaging method). The shape of the model output (two parametric equations) has the advantage to be simple and easy to implement for resonant NEMS designers. Particularly, the importance of the fifth order nonlinearities has been demonstrated through the analytical as well as experimental identification of the mixed behavior.

REFERENCES

[1] K. L. Ekinci and M. L. Roukes. Nanoelectromechanical systems. *Review of Scientific Instruments*, **76**(6):061101, 2005.

[2] K. L. Ekinci, X. M. H. Huang and M. L. Roukes. Ultrasensitive nanoelectromechanical mass detection. *Appl. Phys. Lett.*, **84**:446971, 2004.

[3] K. Jensen, K. Kim and A. Zettl. An atomic-resolution nanomechanical mass sensor. *Nature Nanotechnology*, **3**, 533–537, 2008.

[4] C. T. Nguyen, Micromechanical components for miniaturized low-power communications. In *In 1999 IEEE MTT-S international Microwave Symposium FR MEMS Workshop*, 48–77, 1999.

[5] C. T.-C. Nguyen, A. C. Wong and D. Hao, Tunable, switchable, high-q vhf microelectromechanical bandpass filters. In *In IEEE International Solid-State Circuits Conference*, **448**, 78–79, 1999.

[6] A. Cho, Physics - researchers race to put the quantum into mechanics. *Science*, **299**(5603), 36–37, 2003.

[7] M. D LaHaye, O. Buu, B. Camarota and K. C. Schwab, Approaching the quantum limit of a nanomechanical resonator. *Science*, **304**, 74–77, 2004.

[8] X. L. Feng, Phase noise and frequency stability of very-high frequency silicon nanowire nanomechanical resonators. In *14th International Conference on Solid-State Sensors, Actuators and Microsystems*, 327–30, 2007.

[9] W. P. Robins, *Phase Noise in Signal Sources*. Institution of Engineering and Technology, 1984.

[10] T. A. Roessig, R. T. Howe, and A. P. Pisano, Nonlinear mixing in surface-micromachined tuning fork oscillators. In *Frequency Control Symposium, 1997., Proceedings of the 1997 IEEE International*, 778–782, May 1997.

[11] V. Kaajakari, J.K. Koskinen, and T. Mattila, Phase noise in capacitively coupled micromechanical oscillators. *Ultrasonics, Ferroelectrics and Frequency Control, IEEE Transactions on*, **52**(12), 2322–2331, Dec. 2005.

[12] N. Kacem, S. Hentz, D. Pinto, B. Reig, and V. Nguyen, Nonlinear dynamics of nanomechanical beam resonators: improving the performance of nems-based sensors. *Nanotechnology*, **20**(27):275501, 2009.

[13] N. Kacem, J. Arcamone, F. Perez-Murano, and S. Hentz, Dynamic range enhancement of nonlinear nanomechanical resonant cantilevers for highly sensitive nems gas/mass sensor applications. *Journal of Micromechanics and Microengineering*, **20**(4):045023, 2010.

[14] N. Kacem, S. Baguet, S. Hentz, and R. Dufour, Computational and quasi-analytical models for non-linear vibrations of resonant mems and nems sensors. *International Journal of Non-Linear Mechanics*, **46**(3):532–542, 2011.

[15] M. R. M. Crespo Da Silva and C. C. Glynn, Nonlinear flexural-flexural-torsional dynamics of inextensional beams. i: Equations of motion. *Journal of Structural Mechanics*, **6**:437448, 1978.

[16] M. R. M. Crespo Da Silva and C. C. Glynn, Nonlinear flexural-flexural-torsional dynamics of inextensional beams. ii: Forced motions. *Journal of Structural Mechanics*, **6**:449461, 1978.

[17] M. R. M. Crespo Da Silva, Non-linear flexural-flexural-torsional-extensional dynamics of beams. i: Formulation. *International Journal of Solids and Structures*, **24**:12251234, 1988.

[18] M. R. M. Crespo Da Silva, Non-linear flexural-flexural-torsional-extensional dynamics of beams. ii: Response analysis. *International Journal of Solids and Structures*, **24**:12351242, 1988.

[19] N. Kacem and S. Hentz, Bifurcation topology tuning of a mixed behavior in nonlinear micromechanical resonators. *Applied Physics Letters*, **95**(18):183104, 2009.